D.M. Freik[1], I.I. Chavyak[1], V.I. Makovishin[1], I.A. Arsenyuk[2]

[1]Vasyl Stefanyk Precarpathian National University, 57, Shevchenko Str., Ivano-Frankivsk, 76018, Ukraine;
[2]Ivan Ohienko Kamyanets-Podilsky National University, 61, Ohienko Str., Kamyanets-Podilsky, 32300, Ukraine

THERMOELECTRIC VAPOUR-PHASE CONDENSATE
OF *P*-TYPE TIN TELLURIDE

Structural and thermoelectric properties of p-SnTe thin films of different thickness d = (40 – 800) nm, prepared by vapour condensation in open vacuum on fresh cleavages (0001) of muscovite mica have been investigated. Based on the statistical analysis of the experimental results, increase in conductivity σ, carrier mobility μ and some reduction of the Seebeck coefficient S and the hole concentration p with growing condensate thickness d has been established. It has been shown that maximum specific thermoelectric power $S^2\sigma$ is ~ 18 μW/K, which is important for creation of p-legs of thermoelectric micromodules. The stable p-type conductivity has been attributed to tin vacancies in the cation sublattice of SnTe crystal structure.

Key words: thin films, tin telluride, structure, thermoelectric properties, defects.

Introduction

Tin telluride *SnTe* is a narrow-gap ($E_{g300K} \approx 0.2$ eV) semiconductor whose homogeneity region is fully displaced towards chalcogen, which is responsible for high carrier concentration (~ 10^{20} cm^{-3}) and stable *p*-type conductivity (Fig. 1 *a*) [1-2]. *SnTe* is crystallized in *NaCl* structure whose lattice parameter within the homogeneity region (50.1 – 50.9) at.% *Te* is reduced (Fig. 1 *b*) [2-4]. It is established that the predominant defects in *SnTe* crystals are tin vacancies V_{Sn} of different ionization degrees (V_{Sn}^{2-}, V_{Sn}^{4-}). Recalculation of current carrier concentration *p* into atomic fraction of superstoichiometric tellurium can be done according to relationship [1]:

$$(X_{Te} - 0.5 = nM / 4Z\rho N) \approx 7.9325 \cdot 10^{-24} p, \tag{1}$$

where *M* is the molar mass of *SnTe*, *Z* is ionization degree of point defects, ρ is *SnTe* density (ρ = (6.445 ± 0.01) g/cm^3 at 298 K), *N* is the Avogadro number.

From the results of calculations [5-6], when a metal is removed from the cation nodes of crystal lattice *SnTe*, it loses four electrons, and the valence band – only one level, thus leaving two vacant states, resulting in the appearance of two holes in the valence band, so tin vacancy V_{Sn} is an effective acceptor.

With this in mind, both pure *SnTe* [7] and doped with different impurities [8], as well as solid solutions based on tin telluride [3-9, 10] are promising materials for *p*-legs of thermoelements in the medium temperature range (500 – 750) K. As regards thin-film *SnTe* structures, they greatly expand the possibilities of practical application [11-13]. This paper presents the results of research on the structure and thermoelectric properties of tin telluride thin films prepared by vapour-phase deposition in vacuum on mica single crystal substrates.
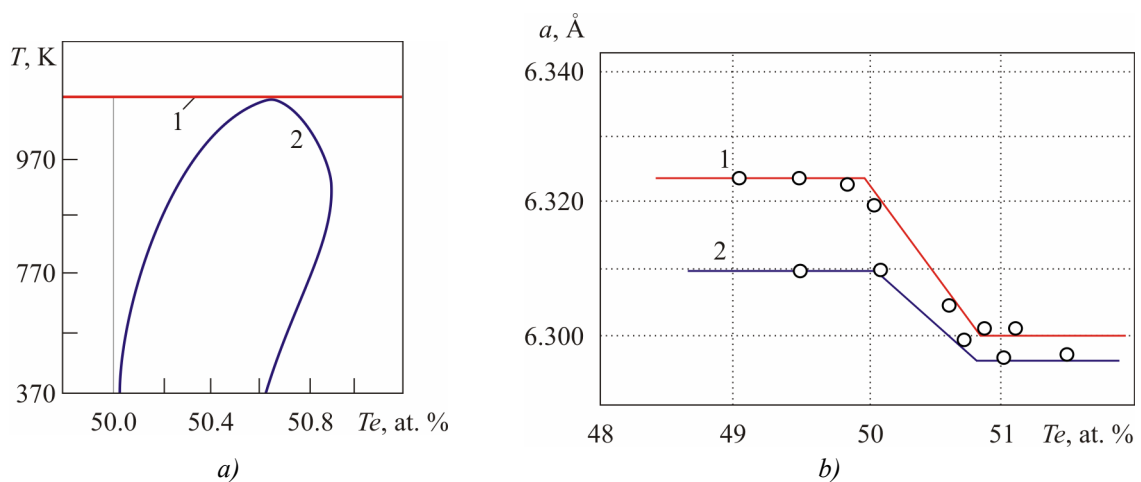
Fig. 1. Homogeneity region boundaries (a): (1 – liquidus, 2 – solidus) and (b): dependences of lattice parameter on tellurium content at T, K: 1 – 673; 2 – 973 in tin telluride (b) [1].

1. Experimental procedure

To obtain a condensate of different thickness d at the assigned deposition temperature T_n, use was made of a vacuum sectional heater with five micro heaters made of vacuum copper rods of size $40 \times 20 \times 8$ mm³ with openings provided for ceramic tubes with heating elements (Fig. 2). From the bottom of the case there is a platform with supports for the substrate. To reduce thermal losses from the surfaces of substrates and to shape the condensate, tantalum screens 0.3 mm thick were installed. All micro heaters were calibrated for equal temperature by selecting the resistance of nichrome wire of diameter 0.3 mm. Heater temperatures are measured by "chromel-copel" thermocouples placed in their cases close to substrates. A system of micro heaters is diagonally fixed to swinging arm, and heating elements are connected in parallel (Fig. 2).
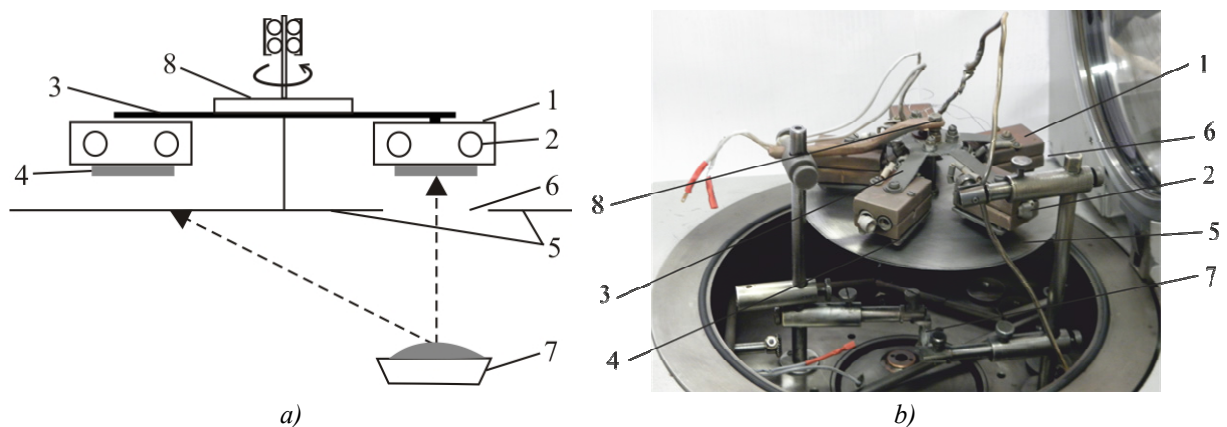

Fig. 2. Structural scheme (a) and picture (b) of sectional heater for preparation of vapour-phase films and nanostructures: 1 – micro heater system, 2 – heaters, 3 – radial arms, 4 – supports for vapour deposition, 5 – gate, 6 – asymmetrically arranged opening, 7 – evaporator, 8 – mechanical microheater pivot system.

Vapour-phase condensates are prepared in the following way (Fig. 2): evaporator 7 is loaded with a weight of substance under study (powder of synthesized tin telluride compound); prepared substrates 4 (fresh mica cleavages) are placed into heaters 1; with closed gate 5 micro heaters 1 with substrates 4 and evaporator with weight 7 are heated to assigned temperature; one of the heaters is brought under opening 6 in the gate above evaporator 7 and vapour is deposited on the substrate for a

certain fixed period; then vapour flow from the evaporator is closed with the gate, the next of sectional micro heaters with a substrate is pivoted, the gate is opened and deposition of a different duration is performed. The above process is repeated five times for each micro heater with substrates.

In our case, *SnTe* vapour was deposited on fresh cleavages (0001) of muscovite mica at weight evaporation temperature $T_e = 870$ K, the temperature of substrates (deposition) $T_s = 470$ K and different deposition periods $\tau = 5 - 360$ s, which assured condensate thicknesses within $d = 40 - 800$ nm.

The obtained nanostructures were studied by atomic force microscopy (AFM) methods Nanoscope 3a Dimension 3000 (Digital Instruments USA) in periodic contact mode. Measurements were performed in the central part of the samples using serial silicone probes NSG-11 with a nominal edge bending radius to 10 nm (NT0MDT, Russia). According to the results of AFM studies of vapour-phase condensates, the surface morphology and its profilographs were determined.

The electric parameters of films were measured in the air at room temperatures in constant magnetic fields on the elaborated automated installation that provides for measurement of electric parameters, as well recording and primary data processing, with the possibility of constructing the plots of temporal and temperature dependences. The sample under measurement had four Hall and two current contacts. As the ohmic contacts, silver films were used. Current through the samples was ≈ 1 mA. The magnetic field was directed normal to the surface of films at induction 1.5 T.

The results of AFM studies and the thickness dependences of electric conductivity σ, the Seebeck coefficient S and thermoelectric power $S^2\sigma$, as well as the Hall coefficient R_H, hole concentration p and their mobility μ for *p-SnTe* films are depicted in Fig. 3 – 4.

2. Experimental results and their analysis
2.1. Condensate structure

Analysis of AFM-studies (Fig. 3) indicates that deposition temperature T_s and deposition time τ are important technological factors that determine the mechanisms of *SnTe* nanocrystals growth on cleavages (0001) of muscovite mica with vapour deposition in open vacuum, their topology and dimensions. The general symptom, under conditions of optimal evaporation temperatures $T_e = 870$ K and deposition temperature $T_s = 470$ K, is the fact that with increasing the deposition time τ (thickness d), the shape and dimensions of individual nanoformations are changed (Fig. 3). Thus, in particular, individual nanoformations are formed with a tendency to cubic forms with lateral dimensions growing with increase in deposition time from ~ 250 nm ($\tau = 5$ s) to ~ 400 nm at $\tau = 10$ s and ~ 700 nm at $\tau = 210$ s, respectively (Fig. 3). In so doing, the height of nanostructures is reduced from ~ 25 nm to 18 and 9 nm, respectively for $\tau = 5$, 10 and 210 s (Fig. 3-II). The most pronounced cubic form of nanostructures takes place at deposition time $\tau = 10$ s (Fig. 3-I, *b*). In so doing, during the late growth stages there is a predominant orientation of nanocrystals with cube edges {100} parallel to substrate surface and their considerable disorientation (Fig. 3-I). However, during the initial growth stages there is orientation effect of substrate which causes formation of pyramidal structures with typical orientation (111) of *SnTe*/(0001) mica (Fig. 3-1, *a*).

Note that with the heteroepitaxial growth there are three different nucleation mechanisms [14]: the Frank-van der Merve mechanism, when layer-by-layer (two-dimensional) material growth of condensate *B* takes place on substrate *A*; the Volmer-Weber mechanism, when island-type (three-dimensional) growth of *B* takes place on the open surface of substrate *A*; the Stransky-Krastanow mechanism, when, at first, layer-by-layer growth of *B* on *A* is realized with subsequent formation of three-dimensional islands *B* on the substrate already coated with condensate.
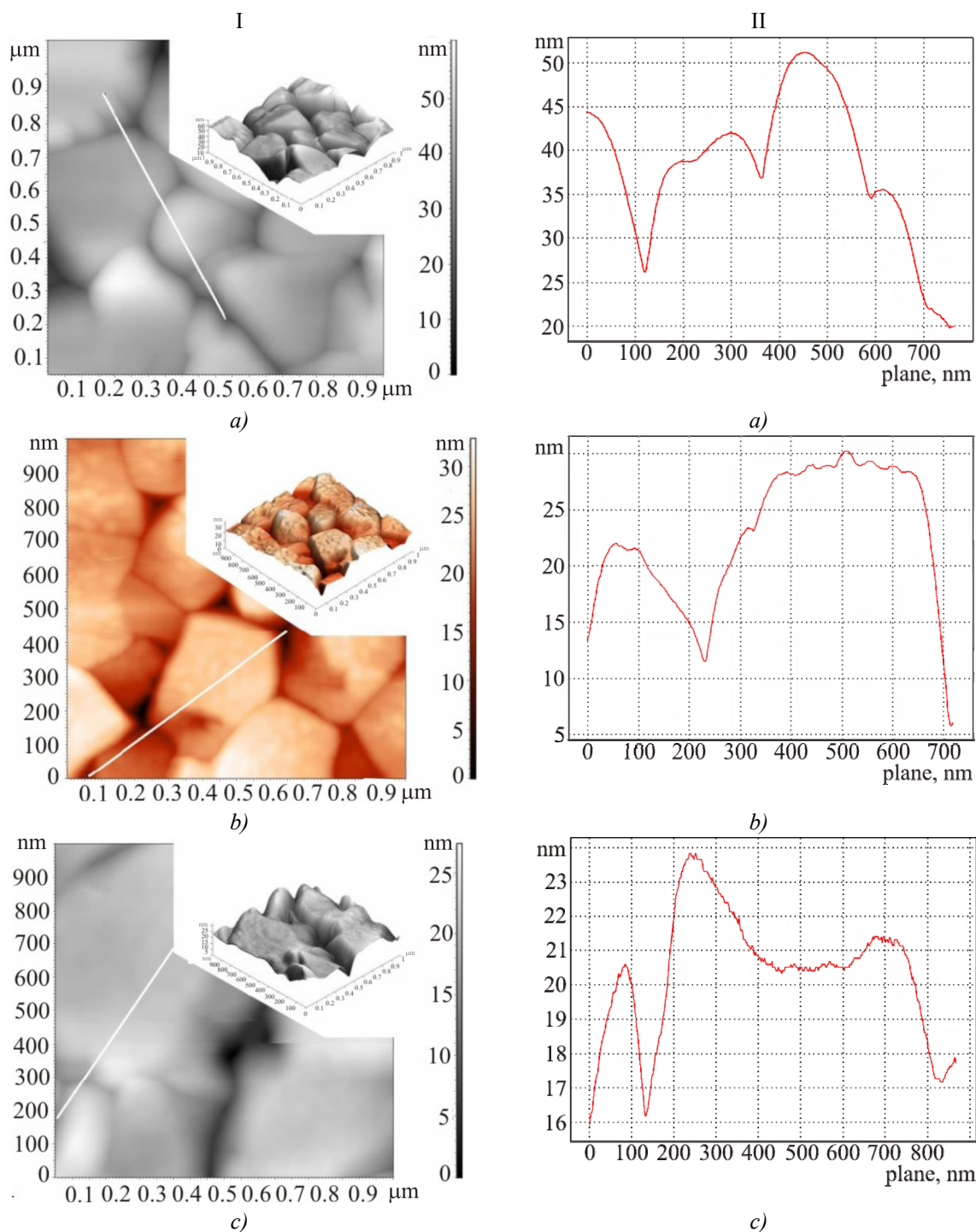
Fig. 3. 2D and 3D AFM images (I) and profilographs (II) of vapour-phase condensates SnTe/(0001) muscovite mica with different vapour deposition times τ,s: a – 5; b – 10; c – 210.

Realization of the former two mechanisms is determined by the energy ratio of the two surfaces (E_B, E_A) and the interface energy E_{BA}. If the sum of surface energy of epitaxial layer E_B and interface energy E_{BA} is smaller than the surface energy of substrate $E_B + E_{BA} < E_A$, that is, when substrate is wetted by condensate, then the Frank-van der Merve mechanism is realized. A change in $E_B + E_{BA}$ value can result in transition from the Frank-van der Merve mode to the Volmer-Weber mode. With certain mismatch in lattice constant between condensate and substrate, there occurs formation of isolated islands through relaxation of elastic stresses which is typical of the Stransky-Krastanow mode.

In our case, the heteroepitaxial growth of *SnTe*/(0001) muscovite mica nanostructures is realized by the Volmer-Weber mechanism according to which individual nanocrystals with certain topological architecture are formed (Fig. 3).

2.2. Thermoelectric properties

It has been established that all *SnTe* films, irrespective of their preparation conditions, are characterized by *p*-type conductivity. In so doing, as is evident from Fig. 4 *a*, with increase in condensate thickness (d), conductivity (σ) increases with attainment of saturation and already at $d \approx 600$ nm reaches considerable values $\sigma = (5 - 8) \cdot 10^3\, \Omega^{-1} \mathrm{cm}^{-1}$ The Seebeck coefficient also increases to the value of $S = 70 - 75\, \mu V/K$, but with reduction in condensate thickness $d < 100$ nm (Fig. 4, *b*). Such values cannot be reached for the bulk samples [1]. For thick films it does not depend on thickness and is $S \approx 40\, \mu V/K$. Based on the obtained values of $\sigma(d)$ and $S(d)$ (Fig. 4, *a*, *b*), a dependence of power factor $P = S^2\sigma$ on *SnTe* thickness in condensate *p-SnTe*/(0001) mica was determined (Fig. 4, *c*). Here also one can see growth of thermoelectric power factor with a decrease in thickness which is $P \approx 18\, \mu W/K^2 \mathrm{cm}$ at $d < 100$ nm (Fig. 4, *c*).
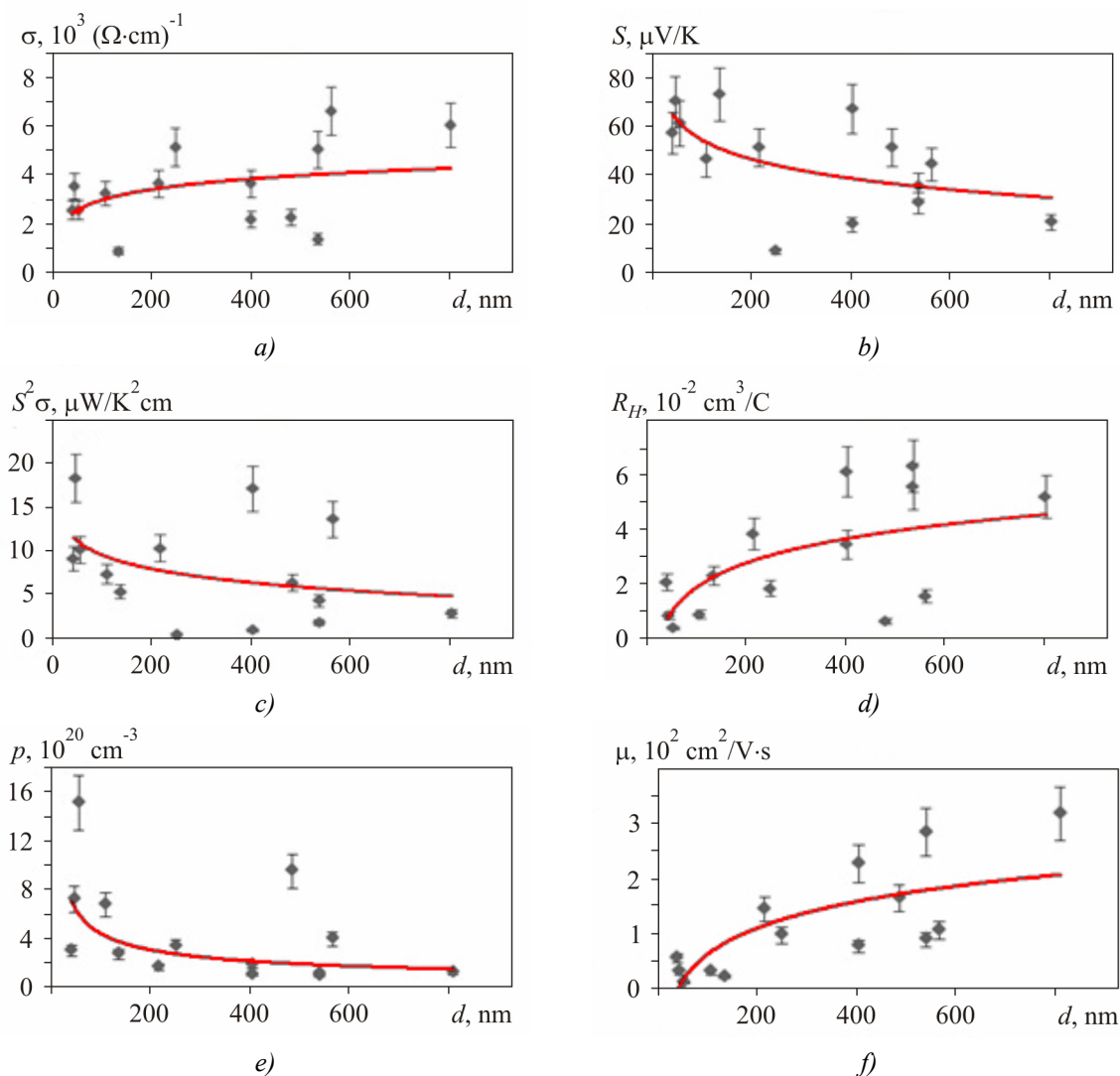

Fig. 4. Dependence of thermoelectric parameters (a – electric conductivity σ*, b – the Seebeck coefficient S, c – thermoelectric power* $S^2\sigma$*, d – the Hall coefficient* R_H*, e – carrier concentration p, f – mobility* μ *on the thickness of vapour-phase condensates SnTe/(0001) muscovite mica.*
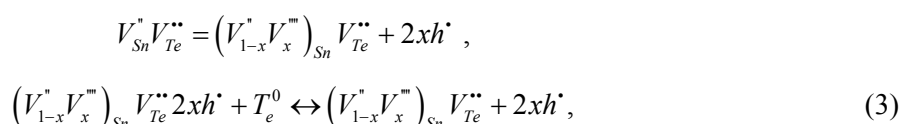
As regards other kinetic coefficients (the Hall concentration p and carrier mobility μ), their thickness dependences have the opposite character of changes: with increase in condensate thickness hole concentration decreases (Fig. 4, *c*), and mobility increases (Fig. 4, *f*). Note that the dominant role in the thickness dependence σ(*d*) of condensates is played in our case by mobility (σ = *qp*μ, where *q* is an elementary charge) (Fig. 4, *a, f*), rather than by carrier concentration p (Fig. 4, *a, e*).

3. Crystal chemistry of defective systems

The experimentally observed stable *p*-type conductivity and high intrinsic concentration of charge carriers in vapour-phase nonstoichiometric *p-SnTe* condensate in terms of crystal-chemical approach is related to completion of anion sublattice and formation of tin vacancies V_{Sn} of crystal structure [15]. Thus, in the case of existence of only two-charge tin vacancies V_{Sn}^{2-} crystal-chemical cluster will be presented as
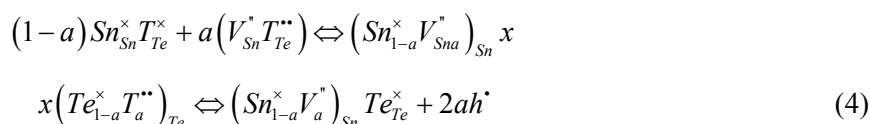
$$V_{Sn}^{''}T_{e}^{\bullet\bullet} + T_{e}^{0} \leftrightarrow V_{Sn}^{''}T_{Te}^{\bullet\bullet}, \tag{2}$$

and in the presence of two- V_{Sn}^{2-} and four-charge V_{Sn}^{4-} vacancies

$$V_{Sn}^{''}V_{Te}^{\bullet\bullet} = \left(V_{1-x}^{''}V_{x}^{'''}\right)_{Sn}V_{Te}^{\bullet\bullet} + 2xh^{\bullet},$$

$$\left(V_{1-x}^{''}V_{x}^{'''}\right)_{Sn}V_{Te}^{\bullet\bullet}2xh^{\bullet} + T_{e}^{0} \leftrightarrow \left(V_{1-x}^{''}V_{x}^{'''}\right)_{Sn}V_{Te}^{\bullet\bullet} + 2xh^{\bullet}, \tag{3}$$

respectively.

Here, " $''$ ", " $\bullet\bullet$ ", "0" are positive, negative and neutral charges, $h^{\bullet}$ – hole, x – fraction of V_{Sn}^{4-}.

The superposition of the resulting clusters with crystal-chemical formula $Sn_{Sn}^{\times}T_{Te}^{\times}$ yields crystal-quasi-chemical formula of nonstoichiometric tin telluride:

$$(1-a)Sn_{Sn}^{\times}T_{Te}^{\times} + a\left(V_{Sn}^{''}T_{Te}^{\bullet\bullet}\right) \Leftrightarrow \left(Sn_{1-a}^{\times}V_{Sna}^{''}\right)_{Sn}x$$

$$x\left(Te_{1-a}^{\times}T_{a}^{\bullet\bullet}\right)_{Te} \Leftrightarrow \left(Sn_{1-a}^{\times}V_{a}^{''}\right)_{Sn}Te_{Te}^{\times} + 2ah^{\bullet} \tag{4}$$

in the first case (2) and

$$(1-a)Sn_{Sn}^{\times}T_{Te}^{\times} + a\left(V_{1-x}^{''}V_{x}^{'''}\right)_{Sn}Te_{Te}^{\times} + 2xh^{\bullet} \Leftrightarrow$$

$$\Leftrightarrow \left[Sn_{1-a}^{\times}V_{(1-x)a}^{''}V_{xa}^{'''}\right]_{Sn}Te_{Te}^{\times} + 2a(1+x)h^{\bullet} \tag{5}$$

in the second case (3), respectively.

Full electroneutrality equations for crystals with the available charged point defects for (4) and (5) will be as follows:

$$2\left[V_{aSn}^{2-}\right] = 2ap, \tag{6}$$

and

$$2\left[V_{(1-x)aSn}^{2-}\right] + 4\left[V_{xaSn}^{4-}\right] = 2a(1+x)p, \tag{7}$$

respectively.

Here *a* is a deviation from stoichiometry that corresponds to superstoichiometric tellurium in compound; *p* is hole concentration, [ ] are concentrations of respective charged defects.

Calculations performed on the basis of relations (4), (7) indicate that increase in the content of superstoichiometric tellurium in homogeneity region of *SnTe* compound causes increase in the concentrations of two-charge $[V_{Sn}^{2-}]$ (Fig. 5, *a* – curve 1) and four-charge $[V_{Sn}^{4-}]$ (Fig. 5, *a* – curve 2) tin vacancies, as well as in hole concentration (Fig. 5, *b* – curve 1). In so doing, for the values of (50 – 50.4) at.% *Te* the prevalent mechanism is formation of four-charge vacancies $[V_{Sn}^{2-}]$ (Fig. 5, *b* – curve 2), which is also indicated by drastic increase in the number of carriers which falls on one tin vacancy ($Z = p/[V_{Sn}]$ (Fig. 5, *b* – curve 2). In the concentration range (50.4 – 50.9) at.% *Te* the dominant process is formation of two-charge tin vacancies $[V_{Sn}^{2-}]$ (Fig. 5, *a* – curve 1), and the value *Z* varies only slightly (Fig. 5, *b* – curve 2).
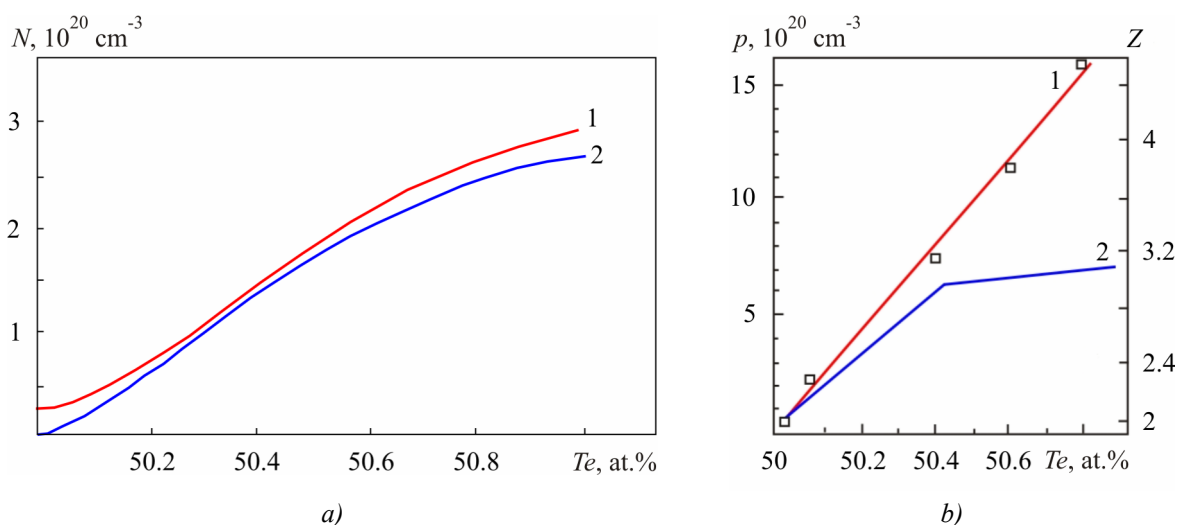

a)   *b)*

Fig. 5. Dependences a): of two-charge 1 – [V_{Sn}^{2-}], four-charge 2 – [V_{Sn}^{4-}] tin vacancies and b): 1 – hole concentration p and carrier number per one tin vacancy Z on tellurium content for SnTe crystals.

With regard to the foregoing, it can be unambiguously asserted that the intrinsic hole concentration in vapour-phase condensates *p-SnTe* is due to a defective subsystem of crystalline structure, namely cation vacancies V_{Sn}. The experimentally observed reduction of carrier concentration with thickness increase (Fig. 4, *e*) can be also due to a change in the value of superstoichiometric tellurium, namely its reduction during evaporation of weight in the evaporator. The latter leads to prevalence of two-charge tin vacancies V_{Sn}^{2-} over tetravalent V_{Sn}^{4-} (Fig. 5, *a*), which is the reason for the Hall concentration decrease.

Conclusions

1. Results of research on the structure and thermoelectric properties of *p-SnTe* thin films of different thickness (40 – 800) nm deposited in open vacuum on fresh cleavages (0001) of muscovite mica are presented.
2. It is shown that vapour-phase condensate is formed by the Volmer-Weber mechanism with formation of individual clusters with (100) and (111) orientations of *SnTe*/(0001) muscovite mica.
3. The thickness dependences of thermoelectric parameters of condensates have been determined. High values of the Seebeck coefficient ($S \approx 70$) µV/K and thermoelectric power $S^2\sigma \approx 18$ µW/K^{2}cm have been revealed that are much in excess of similar parameters for the bulk crystals.

4. The stable *p*-type conductivity and high hole concentration $(10^{20} - 10^{21})$ cm^{-3} has been explained by formation of two-charge and four-charge cation vacancies $(V_{Sn}^{2-}, V_{Sn}^{4-})$ caused by deviation from stoichiometry towards tellurium.

References

1. V.M. Shperun, D.M. Freik, V.V. Prokopiv, *Tin Telluride, Physical and Chemical Properties*, Ed. by D.M. Freik (Ivano-Frankivsk: Plai, 2002), 152 p.
2. R.Kh. Achkurin, V.B. Ufimtsev, Calculation of the Boundaries of Homogeneity Range of Lead and Tin Tellurides, *Russian Journal of Physical Chemistry* **53** (6), 1441 – 1445 (1979).
3. N.Kh. Abrikosov, V.F. Bankina, L.V. Poretskaya., E.V. Skudnova, and S.N. Chizhevskaya, *Semiconductor Chalcogenides and Alloys on their Basis* (Moscow: Nauka, 1975), 219 p.
4. L.E. Shelimova, N.Kh. Abrikosov, *Sn-Te* system in the Region of *SnTe* Compound, Russian *Journal of Inorganic Chemistry* **9** (8), 1879 – 1882 (1964).
5. N.Y. Parada, G.W. Preat, New Model for Vacancy States in *SnTe*, *Phys. Rev. Lett*. **22** (5), 180 – 183 (1969).
6. G.W. Prat, Vacancy and Interstitial States in the Lead Salts, Y. Nouwetals **1**, 103 – 109 (1973).
7. E.P. Sabo, Technology of Chalcogenide Thermoelements. Physical Foundations, *J.Thermoelectricity* **4**, 57 – 65 (2003).
8. N.I. Dziubenko, E.I. Rogacheva, V.M. Kosevich, S.A. Laptev, and A.V. Arankin, Effect of Indium, Gallium, Antimony and Bismuth on the Properties of Tin Telluride, *Izvestiya AN SSSR: Inorganic Materials* **19** (9), 1457 – 1461 (1983).
9. N.I. Dziubenko, E.I. Rogacheva, Interaction in *SnTe-GaTe* and *SnTe-Ga₂Te₃* Systems, *Izvestiya AN SSSR: Inorganic Materials* **23** (6), 1736 – 1737 (1987).
10. D.M. Freik, I.M. Ivanishin, Physical and Chemical Properties and Dominant Defects in Crystals of *Sn-Sb-Te*, *Sn-Bi-Te* System, *Physics and Chemistry of Solid State* **7** (3), 289 – 296 (2006).
11. B.S. Dzundza, I.I. Chavyak, A.I. Tkachuk, G.D. Mateik, and O.L. Sokolov, Near-Surafce Layers and Profiles of Electrical Parameters of *SnTe* Thin Films, *Physics and Chemistry of Solid State* **11** (3), 614 – 617 (2010).
12. I.K. Yurchishin, I.I. Chavyak, Yu.V. Lisyuk, and L.T. Kharun, Size Effects in Thermoelectric Parameters of Tin Telluride, *Physics and Chemistry of Solid State* **11** (4), 898 – 903 (2010).
13. I.I. Chavyak, Stannum Telluride Nanostructures on Muscovite Mica Cleavages, *Physics and Chemistry of Solid State* **13** (1), 62 – 68 (2012).
14. B.V. Ivansky, *Ostwald Ripening of Nanostructures under Conditions of Diffusion-Wagner Mass Transport Mechanism, PhD Thesis*, Chernivtsi, 2011, 152 p.
15. M.O. Galuschak, D.M. Freik, I.M. Ivanyshyn, A.V. Lisak, and M.V. Pyts, Thermoelectric Properties and Defective Subsystem in Doped Telluride of Tin, *J. Thermoelectricity* **1**, 43 – 51 (2000).